IEEE Access
Multidisciplinary | Rapid Review | Open Access Journal

Received February 18, 2019, accepted March 16, 2019, date of publication March 26, 2019, date of current version April 12, 2019.

Digital Object Identifier 10.1109/ACCESS.2019.2907531

Advanced Direct Synthesis Approach for High Selectivity In-Line Topology Filters Comprising *N* - 1 Adjacent Frequency-Variant Couplings

YUXING HE[1], (Member, IEEE), GIUSEPPE MACCHIARELLA[2], (Fellow, IEEE), ZHEWANG MA[3], (Member, IEEE), LIGUO SUN[4], AND NOBUYUKI YOSHIKAWA[1], (Senior Member, IEEE)

[1]Institute of Advanced Sciences, Yokohama National University, Yokohama 240-8501, Japan
[2]Dipartimento di Elettronica Informazione e Bioingegneria, Politecnico di Milano, 20133 Milano, Italy
[3]Graduate School of Science and Engineering, Saitama University, Saitama 338-8570, Japan
[4]Department of EE & Information Science, University of Science and Technology of China, Hefei 230027, China

Corresponding author: Yuxing He (he-yuxing-zj@ynu.ac.jp)

ABSTRACT In this paper, a direct synthesis approach is presented to realize high selectivity in-line topology filters with adjacent frequency-variant couplings (FVCs). By considering the annihilation of frequency-variant elements during admittance matrix transformation for the first time, this paper provides a deterministic mechanism (no optimization is involved) that can generate FVCs between every two cascaded resonators. In consequence, a high selectivity filtering response where N–1 transmission zeros are implemented and independently controllable can be achieved for an Nth-order in-line network. As the foundation, a novel matrix process is detailed to obtain two adjacent FVCs inside of a 4th-order in-line network. The Nth-order prototype is then realized based on the process in an iterative manner. A synthesis example is illustrated in terms of the proposed approach step by step to show validity. Eventually, a 6th-order in-line band-pass filter, which contains adjacent FVCs in two pairs has been designed and fabricated via coaxial cavity structures. The synthesis results, EM simulation results, and tested results are well matched with each other, which reveals the effectiveness of the presented method during physical implementation.

INDEX TERMS Filter synthesis, frequency-variant coupling, coupling matrix, transmission zero, microwave filters.

I. INTRODUCTION

To meet the rising requirement of wireless communication systems, high selectivity microwave filter with multiple finite transmission zeros (TZs) is becoming a key component in modern microwave front-end design. In recent years, the employment of frequency-variant coupling (FVC) has attracted attention in designing compact high selectivity filters. Compared with a traditional constant coupling in [1]–[6], the combination of slope parameter (i.e., C) and constant parameter (i.e., M) makes an FVC (assumed as $C \cdot \Omega + M$ in the low-pass Ω domain) *vanish* at a specific frequency, which implies that extra TZs can be implemented for a given filter network [7]–[15]. This particular characteristic has been physically demonstrated by a number of structures, such as suspended stripline [7], resonating iris [8], [9], SIW [10], [11], coaxial cavity [12], [13], and waveguide [14], [15].

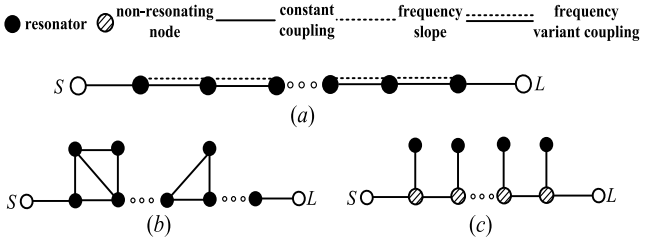

FIGURE 1. Schematic of (a) in-line prototypes discussed in this work (with adjacent frequency-variant couplings); (b) traditional cross-coupled prototypes; and (c) traditional extracted-pole prototypes. Note that solid line (———) refers to traditional constant coupling, dashed line (- - - - -) refers to frequency variant capacitance (slope), and the combination (- - - - -) represents frequency-variant coupling in this work.

Among plenty of efforts, the realization of in-line topology filters that contain FVCs inside, as shown in Fig. 1(a),

The associate editor coordinating the review of this manuscript and approving it for publication was Yongle Wu.

are the most interesting ones [7]–[9], [12], [13]. Instead of applying auxiliary elements such as the cross-coupling pathways (as shown in Fig. 1(b)) [1]–[3] nor non-resonating nodes (as shown in Fig. 1(c)) [4]–[6], TZs here are separately generated by the FVCs between direct-connected resonators, thus showing great advantage in the configuration simplicity. Moreover, the location of each TZ is inherently related to the parameters (C, M) of an FVC [16], which ensures the TZs can be controlled in an independent manner.

On the other hand, synthesis technique for such in-line filters is hardly considered so far. Up to now, it is noticed that most previous designs are on the basis of optimization [17]–[19]. Without a deterministic procedure, one still cannot predict, via a decided in-line network, whether required polynomial responses are realizable. To address this problem, an early contribution on direct synthesis of the mentioned filters is reported in [20]. By applying classical matrix transformations, it is generally proved that a filter containing FVCs is associated with a traditional filter (containing only constant couplings) of the same order. Most recently, an interim method is recommended in [21] and [22], which is adequate to achieve *N/2* finite TZs for an Nth-order in-line filter but cannot satisfy more general situations (where a larger number of TZs is required and adjacent FVCs are involved).

In this paper, an advanced direct approach for synthesizing in-line topology filters containing adjacent FVCs is proposed. In result, it is noted that as many as N - 1 TZs can be achieved for an Nth-order in-line filter (without source-load coupling, this is the maximum TZ number available), which can accommodate most modern communication applications. Specifically, a novel matrix transformation process is introduced to manipulate both mutual couplings and mutual capacitances of a frequency-variant quadruplet. Involving two matrix rotations (with respective rotation angles θ_1 and θ_2) and one rescaling operation (with rescaling factor α), the presented quadruplet is ingeniously reduced to an in-line network once particular relations between the variables (i.e., θ_1, α, and θ_2) are satisfied. In addition, as all the variables are correlated to the initial coupling values in this work, the involved transformations can be described via a single matrix, which distinctly reduces the number of matrix operations and the resulting round-off errors.

In the following, basic admittance matrix transformations are provided in Section II. Afterwards, novel direct synthesis theory for the frequency-variant quadruplet and the Nth-order prototype is detailed in Section III. In Section IV, an 5th-order low-pass prototype with 4 TZs is synthesized to illustrate the effectiveness of the presented approach. Thereafter, we demonstrate a 6th-order in-line band-pass filter containing adjacent FVCs in two pairs by using coaxial cavity structures. Finally, Section VI concludes the paper.

II. ADMITTANCE MATRIX TRANSFORMATION

In this paper, transformations are operated directly to the admittance matrix of an Nth-order low-pass prototype, where

	S	..	i	..	j	..	L
S	1	..	0	..	0	..	0
..	..	..	..	..	..	..	..
i	0	..	$cos\theta$	..	$-sin\theta$	..	0
..	..	..	..	..	..	..	..
j	0	..	$\sin\theta$	..	$cos\theta$	..	0
..	..	..	..	..	..	..	..
L	0	..	0	..	0	..	1

FIGURE 2. Similarity rotation matrix $[R_k]$ (with rotation pivot $[i, j]$ and rotation angle θ), which contains entries $R_{ij} = -R_{ji} = -\sin\theta$, $R_{ii} = R_{jj} = \cos\theta$, and $R_{nn} = 1$ ($n = S, 1, \ldots, N, L, n \neq i, j$).

	S	1	2	..	N-1	N	L
S	1	0	0	..	0	0	0
1	0	$\sqrt{\alpha_1}$	0	..	0	0	0
2	0	0	$\sqrt{\alpha_2}$	..	0	0	0
..	..	..	..	..	..	..	..
N-1	0	0	0	..	$\sqrt{\alpha_{N-1}}$	0	0
N	0	0	0	..	0	$\sqrt{\alpha_N}$	0
L	0	0	0	..	0	0	1

FIGURE 3. Rescaling transformation matrix $[U_k]$, which contains diagonal entries $U_{SS} = U_{LL} = 1$ and respective rescaling parameters $U_{nn} = \sqrt{\alpha_n}$ ($n = 1, 2, \ldots, N$) for the nth resonator.

two basic manipulations, i.e., the similarity rotation and the rescaling transformation, are involved.

Here we briefly recall the established $N + 2$ admittance matrix $[Y] = [M] + \Omega[C] - j[G]$ of an Nth-order prototype [2], [3]. It is known that $[M]$ refers to the frequency-invariant coupling matrix, while $[C]$ describes all the frequency-variant capacitances (slopes) of the prototype. Note that, $[C]$ is diagonal for prototypes with only constant couplings [1]–[6], but changes into non-diagonal when frequency-variant couplings are introduced [20]–[22]. Meanwhile, $[G]$ is the conductance matrix with only two non-zero entries $G_{SS} = G_{LL} = 1$, which reveals the terminal conductances at source and load and remains unchanged during matrix manipulations.

Combining $[M]$ and $[C]$ as an entity, the similarity rotation for $[Y]$ relies on a rotation matrix $[R]$ (pivot assumed as $[i, j]$, shown in Fig. 2), which yields (for the kth rotation)

$$\begin{aligned} [Y_{k+1}] &= [R_{k+1}]\,[Y_k]\,[R_{k+1}]^T \\ [M_{k+1}] &= [R_{k+1}]\,[M_k]\,[R_{k+1}]^T, \quad k = 0, 1, 2, \ldots \\ [C_{k+1}] &= [R_{k+1}]\,[C_k]\,[R_{k+1}]^T \end{aligned} \tag{1}$$

Note that, since non-diagonal entries may exist in the matrix $[C_k]$ in this work, the manipulation in (1) affects both frequency-invariant and frequency-variant coefficients of a filter, which is the main difference with respect to traditional filter synthesis techniques [1]–[3].

Moreover, the rescaling transformation manages capacitances directly. As illustrated in Fig. 3, a rescaling matrix $[U]$ is introduced which contains diagonal rescaling parameters α_n for the nth resonator, thus revealing the following equations in (2).

$$\begin{aligned} [Y_{k+1}] &= [U_{k+1}]\,[Y_k]\,[U_{k+1}]^T \\ [C_{k+1}] &= [U_{k+1}]\,[C_k]\,[U_{k+1}]^T, \quad k = 0, 1, 2, \ldots \\ [M_{k+1}] &= [U_{k+1}]\,[M_k]\,[U_{k+1}]^T \end{aligned} \tag{2}$$

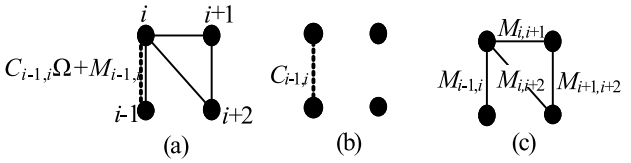

FIGURE 4. (a) Proposed frequency-variant quadruplet with one FVC between resonator i - 1 and i. (b) Its separated frequency-variant part. (c) Its separated frequency-invariant part.

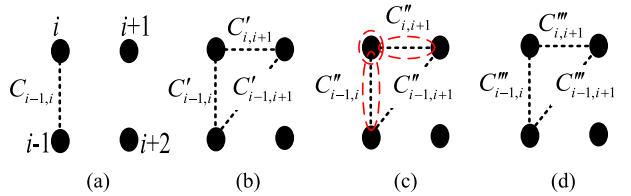

FIGURE 5. Proposed transformation process for the frequency-variant part (capacitances) of the quadruplet. (a) Initial topology; (b) topology after similarity rotation with pivot $[i, i+1]$ and angle θ_1; (c) topology after rescaling at resonator i; and (d) topology after similarity rotation with pivot $[i, i+1]$ and angle θ_2.

As a result, the varied entries of the nth row (or column) of the transformed matrix (i.e., $[C_{k+1}]$ and $[M_{k+1}]$) are calculated by

$$\begin{aligned} C'_{nn} &= \alpha_n C_{nn}, \quad C'_{nk} = C'_{kn} = \sqrt{\alpha_n} C_{nk} = \sqrt{\alpha_n} C_{kn} \\ M'_{nn} &= \alpha_n M_{nn}, \quad M'_{nk} = M'_{kn} = \sqrt{\alpha_n} M_{nk} = \sqrt{\alpha_n} M_{kn} \end{aligned} \tag{3}$$

III. SYNTHESIS THEORY

A. TRANSFORMATION PROCESS OF A FREQUENCY-VARIANT QUADRUPLET

Specifically, a frequency-variant quadruplet which consists of an in-line FVC and a traditional triplet structure, as Fig. 4(a) depicts, is taken into consideration. Note that, the mutual frequency-variant coupling exists initially between resonator i-1 and i (i.e., $C_{i-1,i}\Omega + M_{i-1,i}$), which is different and more general with respect to [21] and [22].

To better demonstrate the process, the frequency-variant quadruplet is separated into frequency-variant part (see Fig. 4(b)) and frequency-invariant part (see Fig. 4(c)) in this section. In order to obtain an in-line topology, both parts should be properly managed at the same time during the following transformations.

Firstly, a similarity rotation is carried out, with pivot $[i, i+1]$ and rotation angle θ_1 (which represents the first rotation angle of the manipulation sequence), for the frequency-variant quadruplet. Assuming the rotation matrix as $[R_1]$, it can be found in Fig. 5(b) that additional mutual capacitances are obtained (e.g., between resonator i-1 and $i+1$, resonator i and $i+1$) after the rotation. In terms of (1), the respective capacitances are decided as

$$\begin{aligned} C'_{i-1,i} &= \cos\theta_1 C_{i-1,i}, \quad C'_{i-1,i+1} = \sin\theta_1 C_{i-1,i} \\ C'_{i,i+1} &= \sin\theta_1 \cos\theta_1 (C_{ii} - C_{i+1,i+1}) \\ C'_{ii} &= \cos^2\theta_1 C_{ii} + \sin^2\theta_1 C_{i+1,i+1} \\ C'_{i+1,i+1} &= \sin^2\theta_1 C_{ii} + \cos^2\theta_1 C_{i+1,i+1} \end{aligned} \tag{4}$$

Additionally, the constant couplings are also affected, which results in:

$$\begin{aligned} M'_{i-1,i} &= \cos\theta_1 M_{i-1,i}, \quad M'_{i-1,i+1} = \sin\theta_1 M_{i-1,i} \\ M'_{i,i+2} &= \cos\theta_1 M_{i,i+2} - \sin\theta_1 M_{i+1,i+2}, \\ M'_{i+1,i+2} &= \sin\theta_1 M_{i,i+2} + \cos\theta_1 M_{i+1,i+2} \\ M'_{ii} &= \cos^2\theta_1 M_{ii} + \sin^2\theta_1 M_{i+1,i+1} - 2\sin\theta_1\cos\theta_1 \\ M'_{i+1,i+1} &= \sin^2\theta_1 M_{ii} + \cos^2\theta_1 M_{i+1,i+1} + 2\sin\theta_1\cos\theta_1 \\ M'_{i,i+1} &= M_{i,i+1}(\cos^2\theta_1 - \sin^2\theta_1) \\ &\quad + \sin\theta_1\cos\theta_1 (M_{ii} - M_{i+1,i+1}) \end{aligned} \tag{5}$$

The obtained schematic of the frequency-invariant part is provided in Fig. 6(b).

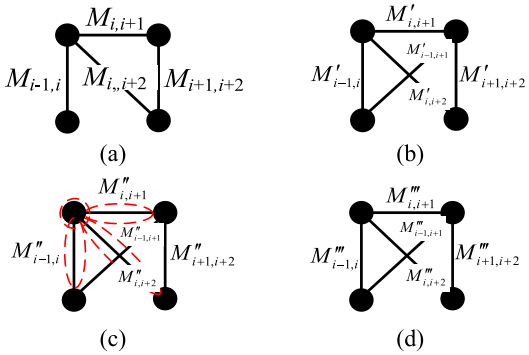

FIGURE 6. Proposed transformation process for the frequency-invariant part (constant couplings) of the quadruplet. (a) Initial topology; (b) topology after similarity rotation with pivot $[i, i+1]$ and angle θ_1; (c) topology after rescaling at resonator i; and (d) topology after similarity rotation with pivot $[i, i+1]$ and angle θ_2.

Thereafter, a rescaling transformation, viz. $[U_1]$, is applied for resonator i, with the rescaling parameter designated as α_i. By means of (2) and (3), the capacitance and constant coupling parameters associated with resonator i will be modified, while the other parameters remain the same. Particularly, the related capacitance parameters are determined as

$$\begin{aligned} C''_{ii} &= \alpha_i C'_{ii}, \quad C''_{i-1,i} = \sqrt{\alpha_i} C'_{i-1,i}, \quad C''_{i,i+1} = \sqrt{\alpha_i} C'_{i,i+1} \\ C''_{i+1,i+1} &= C'_{i+1,i+1}, \quad C''_{i-1,i+1} = C'_{i-1,i+1} \end{aligned} \tag{6}$$

while the corresponding constant couplings become

$$\begin{aligned} M''_{i-1,i} &= \sqrt{\alpha_i} M'_{i-1,i}, \quad M''_{i,i+1} = \sqrt{\alpha_i} M'_{i,i+1}, \\ M''_{i,i+2} &= \sqrt{\alpha_i} M'_{i,i+2} \\ M''_{i-1,i+1} &= M'_{i-1,i+1}, \quad M''_{i+1,i+2} = M'_{i+1,i+2} \\ M''_{ii} &= \alpha_i M'_{ii}, \quad M''_{i+1,i+1} = M'_{i+1,i+1} \end{aligned} \tag{7}$$

The decided network after rescaling is given in separate parts, as provided in Fig. 5(c) and Fig. 6(c).

Finally, one more similarity rotation matrix $[R_2]$ is applied, with pivot $[i, i+1]$ again, to manipulate the frequency-variant capacitances and the frequency-invariant couplings of the quadruplet. Stipulating the rotation angle here as θ_2, the mutual capacitances $C'''_{i-1,i+1}$ and $C'''_{i,i+1}$ thus turn

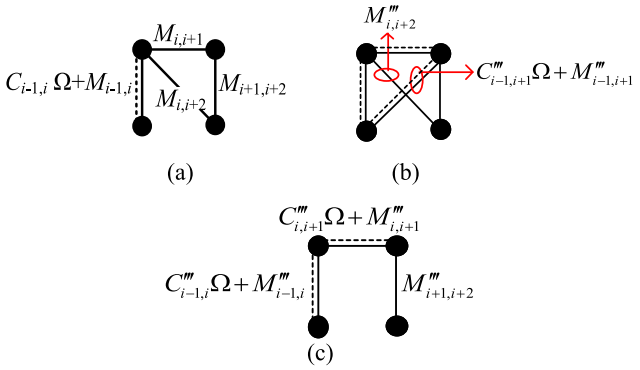

FIGURE 7. Initial frequency-variant quadruplet considered in this work. (b) General topology after presented transformation process. (c) Ultimate 4th-order in-line prototype containing two adjacent FVCs.

out to be

$$\begin{aligned} C'''_{i-1,i+1} &= \sin\theta_2 C''_{i-1,i} + \cos\theta_2 C''_{i-1,i+1} \\ C'''_{i,i+1} &= C''_{i,i+1}(\cos^2\theta_2 - \sin^2\theta_2) \\ &\quad + \sin\theta_2\cos\theta_2(C''_{ii} - C''_{i+1,i+1}) \end{aligned} \tag{8}$$

The corresponding frequency-variant part is illustrated in Fig. 5(d). It can be known from (8) that the rotation here does not introduce extra mutual capacitances but changes the values of $C'''_{i-1,i+1}$ and $C'''_{i,i+1}$.

On the other hand, the frequency-invariant part is also varied where the new parameters $M'''_{i,i+1}$,$M'''_{i-1,i+1}$, and $M'''_{i,i+2}$ become (as shown in Fig. 6(d))

$$\begin{aligned} M'''_{i,i+1} &= M''_{i,i+1}(\cos^2\theta_2 - \sin^2\theta_2) \\ &\quad + \sin\theta_2\cos\theta_2(M''_{ii} - M''_{i+1,i+1}) \\ M'''_{i-1,i+1} &= \sin\theta_2 M''_{i-1,i} + \cos\theta_2 M''_{i-1,i+1} \\ M'''_{i,i+2} &= \cos\theta_2 M''_{i,i+2} - \sin\theta_2 M''_{i+1,i+2} \end{aligned} \tag{9}$$

Based on above manipulations, the ultimate topology of the proposed quadruplet is determined as Fig. 7(b) depicts. Note that, as a general case, the determined quadruplet involves more cross couplings and mutual capacitances. Specifically, mutual couplings $M'''_{i-1,i+1}$, $M'''_{i,i+2}$, and mutual slope $C'''_{i-1,i+1}$ can finally be expressed using (4)-(9) as a function of θ_1, α_i, and θ_2 by:

$$\begin{aligned} C'''_{i-1,i+1} &= \sqrt{\alpha_i}\sin\theta_2\cos\theta_1 C_{i-1,i} + \cos\theta_2\sin\theta_1 C_{i-1,i} \\ M'''_{i-1,i+1} &= \sqrt{\alpha_i}\sin\theta_2\cos\theta_1 M_{i-1,i} + \cos\theta_2\sin\theta_1 M_{i-1,i} \\ M'''_{i,i+2} &= \cos\theta_2(\sqrt{\alpha_i}\cos\theta_1 M_{i,i+2} - \sqrt{\alpha_i}\sin\theta_1 M_{i+1,i+2}) \\ &\quad - \sin\theta_2(\sin\theta_1 M_{i,i+2} + \cos\theta_1 M_{i+1,i+2}) \end{aligned} \tag{10}$$

We observe that the final desired in-line topology (shown in Fig. 7(c)) is obtained by imposing the elements $M'''_{i-1,i+1}$, $M'''_{i,i+2}$, and $C'''_{i-1,i+1}$ equal to zero. The achievement of this goal is discussed in the next paragraph.

B. GENERATION OF A 4TH-ORDER IN-LINE TOPOLOGY

Imposing the elements in (10) equal to zero, we have three equations with the unknown variables θ_1, α_i, and θ_2. However, after inspecting the mentioned equations, it turns out that the three variables are not independent with each other. In particular, we can relate α_i and θ_1 as follows:

$$\alpha_i = -\tan\theta_1 \frac{\sin\theta_1 M_{i,i+2} + \cos\theta_1 M_{i+1,i+2}}{\cos\theta_1 M_{i,i+2} - \sin\theta_1 M_{i+1,i+2}} \tag{11}$$

Then θ_2 can be expressed as function of α_i and θ_1 by:

$$\theta_2 = \tan^{-1}\left(-\frac{\tan\theta_1}{\sqrt{\alpha_i}}\right) \tag{12}$$

The equations (11) and (12) show that we can obtain the desired condition (i.e., elements in (10) equal to zero) by selecting an arbitrary value for θ_1 and determining with (11) and (12) the other unknowns. Note that, the chosen value of θ_1 must however ensure $\alpha_i > 0$ during manipulation.

Once the above three variables have been determined, we can express the overall admittance matrix $\left[Y'''\right]$ of the in-line resulting topology with FVCs from initial matrix $[Y]$ as:

$$\left[Y'''\right] = [T][Y][T]^T \tag{13a}$$

where $[T] = [R_2][U_1][R_1]$ is matrix of order $N+2$ with the following entries

$$\begin{aligned} T_{ii} &= \sqrt{\alpha_i}\cos\theta_1\cos\theta_2 - \sin\theta_1\sin\theta_2 \\ T_{i,i+1} &= -\sqrt{\alpha_i}\sin\theta_1\cos\theta_2 - \cos\theta_1\sin\theta_2 \\ T_{i+1,i} &= \sqrt{\alpha_i}\cos\theta_1\sin\theta_2 + \sin\theta_1\cos\theta_2 = 0 \\ T_{i+1,i+1} &= -\sqrt{\alpha_i}\sin\theta_1\sin\theta_2 + \cos\theta_1\cos\theta_2 \\ T_{nn} &= 1, n = 1, 2, \ldots, i-1, i+2, \ldots, N \end{aligned} \tag{13b}$$

With above discussions, a diagram which describes the manipulation to obtain a 4th-order in-line topology is given in Fig. 8.

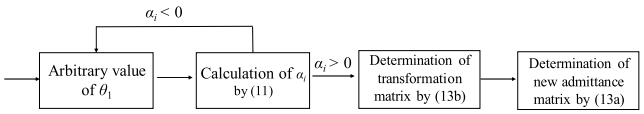

FIGURE 8. Manipulation to obtain a 4th-order in-line topology from a frequency-variant quadruplet in this work.

C. DETERMINATION OF AN NTH-ORDER IN-LINE PROTOTYPE

The generation of an inline topology with adjacent FVCs starts with the synthesis of the wheel canonical prototype [1] of order N depicted in Fig. 9(a), which is assumed to exhibit N - 1 TZs. Using the procedure outlined in [1], a new coupling is added to the prototype, extracting one of the assigned TZ. This coupling is then moved along the wheel by means of suitable similarity rotations (the same used in [1]) until it arrives between resonator 1 and 3, as Fig. 9(b) shows. In this figure, we can identify (inside the dashed line) the same quadruplet considered in Sec. III-B (despite that coupling S-1 is constant as a particular case of Fig. 4(a)), to which the matrices manipulations previously illustrated in (13) can be applied.

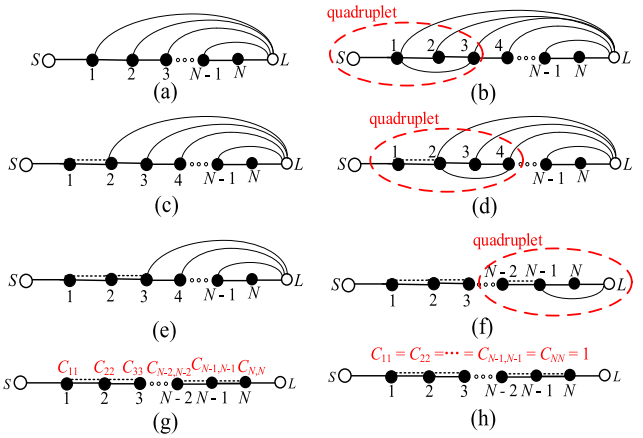

FIGURE 9. Synthesis procedure for an N th-order in-line prototype with N-1 adjacent FVCs. (a) Initial prototype in a wheel canonical topology; (b) prototype containing a frequency-invariant quadruplet among source, resonator 1, 2, and 3; (c) prototype containing an in-line FVC and a wheel topology of N - 1 order; (d) prototype containing a frequency-variant quadruplet among resonator 1, 2, 3, and 4 ; (e) prototype containing two FVCs and a wheel topology of N - 2 order; (f) prototype containing N - 2 FVCs and the last frequency-variant quadruplet; (g) in-line prototype with different capacitance for each resonator; and (h) ultimate in-line prototype with unitary capacitance for each resonator.

It is however noted that additional couplings appear in this quadruplet, which do not exist in the one previously considered (i.e. between load and resonator 1, load and resonator 2). Although these couplings are actually modified by the applied manipulations, they do not affect the couplings inside the quadruplet. In result, by applying (13a) to the whole prototype admittance matrix, the new topology is derived and reported in Fig. 9(c), where an FVC has appeared between resonator 1 and 2, while the coupling between load and resonator 1 (coupling 1-L) disappears. The reason of coupling 1-L vanishing is that the new topology is constituted by the FVC (extracting the originally selected zero) in cascade with a reduced by one order wheel configuration. This latter includes the remaining N - 2 TZs, which infers that the coupling 1-L cannot be present (otherwise the number of TZ is N - 1).

The above described operations represent the first step of an iterative procedure, which proceeds as follows ($i = 1$ at the beginning):

a) Extraction of one TZ from the wheel and moving the generated coupling up to the position between resonator i and $i + 2$, such as depicted in Fig. 9(d).
b) Transformation of the quadruplet with FVC (see Fig. 9(d)) into the in-line block (see Fig. 9(e)) by means of (13a) and (13b). The variables $\theta_{1,i}$, α_i, and $\theta_{2,i}$ are determined through (11)-(12) for the ith FVC generation.
c) Utilization of a) and b) iteratively until $i = N$ - 1, which results in the last quadruplet as Fig. 9(f) exhibits. The prototype with an entire in-line topology is then obtained (Fig. 9(g)) by applying once more the transformation (13a). Note that the elements in the main diagonal of $[C]$ after this step are generally different from one, and the resultant $C_{i,i+1}$ and $M_{i,i+1}$ of the ith FVC will vary when different value of $\theta_{1,i}$ is stipulated during the iterative process.
d) To facilitate the physical implementation of the derived in-line prototype, a final rescaling can be applied to get all the diagonal capacitance unitary (Fig. 9(h)). The rescaling matrix $[U_{final}]$ is reported as:

$$[U_{final}] = \begin{bmatrix} 1 & 0 & 0 & \dots & \dots & 0 \\ 0 & \sqrt{\alpha_1} & 0 & \dots & \dots & 0 \\ 0 & 0 & \sqrt{\alpha_2} & 0 & \dots & 0 \\ \dots & \dots & 0 & \dots & \dots & \dots \\ 0 & \dots & \dots & \dots & \sqrt{\alpha_N} & 0 \\ 0 & 0 & 0 & \dots & 0 & 1 \end{bmatrix}_{N+2,N+2}, \tag{14}$$

with α_i given by

$$\alpha_n = \frac{1}{C_{nn}}, n = 1, 2, \dots, N \tag{15}$$

Stipulating the capacitance of each resonator to be unitary, the final values of $C_{i,i+1}$ and $M_{i,i+1}$ are fixed and not correlated with $\theta_{1,i}$ any more.

Additionally, it is declared that the TZs of the resultant network are generated and controlled by each FVC independently, without using any cross-coupled nor extracted-pole structure. Considering the manipulation and annihilation of FVCs for the first time, the number of TZs realizable for an in-line network is distinctly increased in this work when compared with previous ones.

D. DISCUSSION & COMPARISON WITH LITERATURE

It should be indicated that the proposed transformation is also valid when the initial coupling between resonator i - 1 and i in Fig. 4(a) is constant (i.e., $C_{i-1,i} = 0$, which is the particular case discussed in [22]). According to (10), $C'''_{i-1,i+1}$ after manipulations is fixed to zero here, which does not affect the variable determinations.

On the other hand, (11) and (12) also clarify the limitation of previous method in the literature. Without a correlative equation, i.e., (11), the value of θ_1 in [21] and[22] is specified by annihilating $M_{i,i+1}$ during midterm transformations. In result, the corresponding variable α_i may turn out to be a negative value, which thus prevents the further matrix manipulations and in-line topology simplification.

IV. ILLUSTRATIVE EXAMPLE

To show the effectiveness of the proposed theory, an illustrative fifth-order 26-dB return loss low-pass prototype with quasi-canonical response (exhibiting four TZs) is provided in this section. Particularly, the required TZs are located at $f_{z1} = -1.7j, f_{z2} = 1.5j, f_{z3} = 2j$, and $f_{z4} = 3j$. According to the proposed theory, a quadruplet among source and resonator 1, 2, 3 is firstly derived in Fig. 10(a), where the coupling between resonator 1 and 3 now generates the TZ at f_{z1}. Afterwards, the proposed transformation is applied (with $\theta_{1,1} = -30°$, $\alpha_1 = 0.2060$, and $\theta_{2,1} = 51.8282°$), which derives

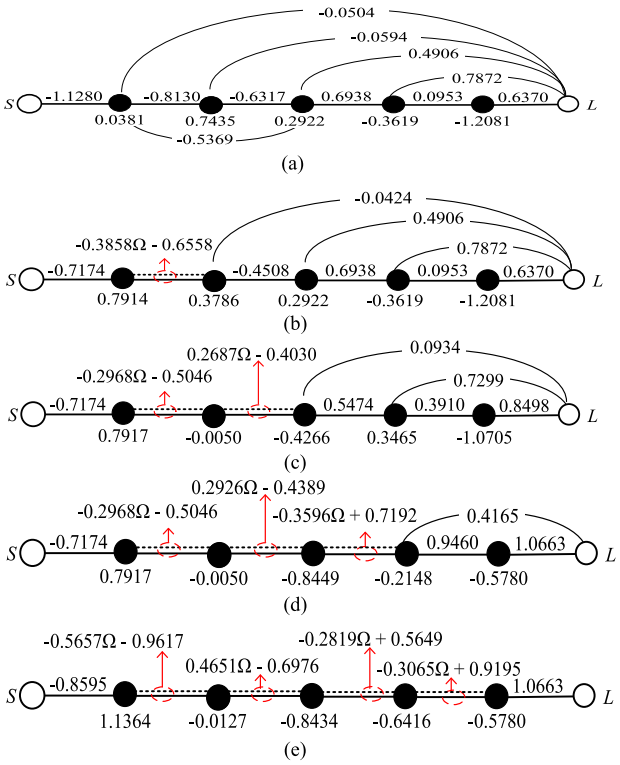

FIGURE 10. Relevant prototypes and coupling coefficients of the fifth-order example. (a) Network containing a quadruplet among source and resonator 1, 2, 3 (capacitances: $C_{11} = C_{22} = C_{33} = C_{44} = C_{55} = 1$); (b) network containing one FVC (capacitances: $C_{11} = 0.6967$, $C_{22} = 0.5093$, $C_{33} = C_{44} = C_{55} = 1$); (c) network containing two FVCs (capacitances: $C_{11} = 0.6967$, $C_{22} = 0.3952$, $C_{33} = 0.7703$, $C_{44} = C_{55} = 1$); (d) network containing three FVCs (capacitances: $C_{11} = 0.6967$, $C_{22} = 0.3952$, $C_{33} = 1.0018$, $C_{44} = 1.4714$, $C_{55} = 1$); (e) ultimate in-line network with four adjacent FVCs (capacitances $C_{11} = C_{22} = C_{33} = C_{44} = C_{55} = 1$).

the first FVC between resonator 1 and 2 (generating f_{z1} at -1.7j), as shown in Fig. 10(b). Moreover, the rest sub-network remains in a wheel-topology, which takes responsibility of f_{z2}, f_{z3}, and f_{z4}.

To obtain an in-line prototype for the whole network, adjacent FVCs located between resonator 2 and 3 (generating f_{z2} at 1.5j), resonator 3 and 4 (generating f_{z3} at 2j), and resonator 4 and 5 (generating f_{z4} at 3j) are determined in Fig. 10(b), (c), and (d) successively by utilizing the iterative procedure mentioned in this paper. The related variables during transformations are given in Table 1. Note that, $\theta_{1,2}$, $\theta_{1,3}$, and $\theta_{1,4}$ are manually selected to ensure positive α_1, α_2, and α_3 by (11). In addition, the particular entries of transformation matrix in each step are calculated from (13b) and listed in Table 2.

The ultimate in-line prototype after rescaling process is introduced in Fig. 10(e), where the capacitances of all resonators are rescaled to unity. It is noticed that the appeared FVC, e.g., coupling 1-2 in Fig. 10(b), 10(c) and 10(e), will be changed during the transformations. However, one can readily observe that the corresponding TZ by such FVC is remained at -(-0.6558/-0.3858) = -(-0.5046/-0.2968) = -(-0.9617/-0.5657) = -1.7j.

TABLE 1. Variables decided for the 5th-order example.

FVC position	*First rotation angle* $\theta_{1,i}$	*Rescaling parameter* α_i	*Second rotation angle* $\theta_{2,i}$
1-2	-30°	0.2060	51.8282°
2-3	30°	0.4561	-40.5274°
3-4	60°	1.7458	-52.6623°
4-5	30°	3.7881	-16.5294°

TABLE 2. Entries of transformation matrix in each step.

i	T_{ii}	$T_{i,i+1}$	$T_{i+1,i}$	$T_{i+1,i+1}$
1	0.6360	-0.5406	0	0.7136
2	0.7695	0.3061	0	0.8777
3	1.0892	-0.2965	0	1.2130
4	1.7581	-0.6867	0	1.1070

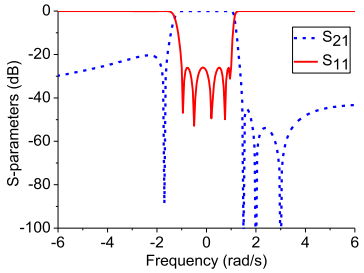

FIGURE 11. Synthesis S-parameters of the fifth-order example.

The corresponding S-parameters of the ultimate in-line prototype perform the desired responses in Fig. 11, thus validating the presented approach.

V. EXPERIMENTAL VALIDATION

For the experimental validation, a 6th-order in-line band-pass filter is demonstrated and manufactured via coaxial cavity structures in this section. To show the flexibility of the presented approach, a filtering response with four TZs is considered here. Specifically, the TZs are generated by directed-coupled FVCs in two pairs: one pair is located among resonator 1-2-3, while the other is among resonator 4-5-6. Detailed requirements are provided as follows: center frequency $f_0 = 1.7825$ GHz, bandwidth $BW = 85$ MHz, return loss 20-dB, and transmission zero locations: $f_{z1} = 1.54$ GHz, $f_{z2} = 1.65$ GHz, $f_{z3} = 1.91$ GHz, $f_{z4} = 2.02$ GHz.

Particularly, f_{z1} (or f_{z2}) is generated by an FVC between resonator 1 and 2 (or between resonator 2 and 3), while f_{z3} (or f_{z4}) is generated by an FVC between resonator 4 and 5 (or between resonator 5 and 6).

A. SYNTHESIS OF THE CORRESPONDING LOW-PASS PROTOTYPE

In terms of frequency normalization process [23], the low-pass prototype of this filter is firstly synthesized by using direct approach proposed in this work. As starting point,

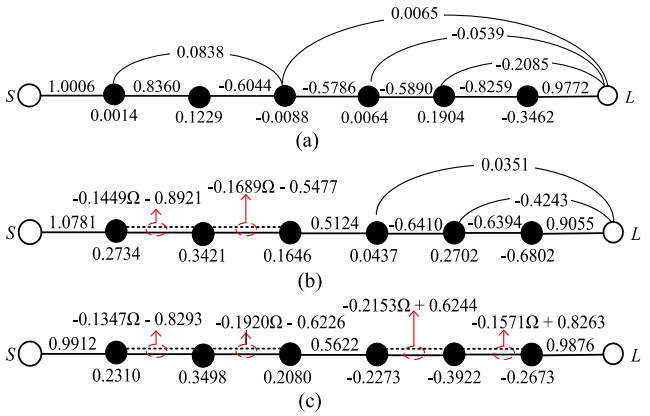

FIGURE 12. Relevant prototypes and coupling coefficients of the sixth-order in-line example. (a) Prototype containing a quadruplet among source and resonator 1, 2, 3 (capacitances: $C_{11} = C_{22} = C_{33} = C_{44} = C_{55} = C_{66} = 1$); (b) Prototype containing two FVCs (capacitances: $C_{11} = 1.1832$, $C_{22} = 0.9780$, $C_{33} = 0.7912$, $C_{44} = C_{55} = C_{66} = 1$); (c) ultimate prototype containing four FVCs (capacitances: $C_{11} = C_{22} = C_{33} = C_{44} = C_{55} = C_{66} = 1$).

TABLE 3. Variables for 6th-order example.

FVC position	*First rotation angle* $\theta_{1,i}$	*Rescaling parameter* α_i	*Second rotation angle* $\theta_{2,i}$
1-2	135°	1.3218	41.0167°
2-3	45°	0.6546	-51.0250°
4-5	60°	0.5430	-66.9524°
5-6	30°	0.7634	-33.4565°

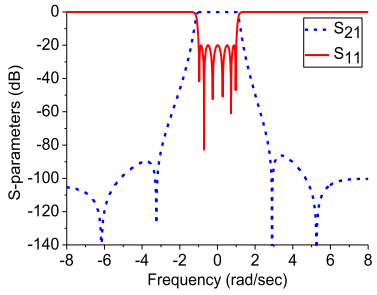

FIGURE 13. Synthesis *S*-parameters of the sixth-order low-pass prototype.

a quadruplet is derived in Fig. 12(a), where the rest sub-network remains in a wheel-topology. Thereafter, two adjacent FVCs are generated for realizing f_{z1} and f_{z2} respectively (as shown in Fig. 12(b)), according to variables listed at the first and second rows of Table 3. Within the same principle, the other two FVCs are then determined successively to realize f_{z3} and f_{z4} by applying variables listed at the third and fourth rows. The ultimate in-line topology is given in Fig. 12(c), where all capacitances have been rescaled to unity. Synthesis results of the derived low-pass prototype are illustrated in Fig. 13, which perform the desired responses.

B. PHYSICAL IMPLEMENTATION

By applying frequency de-normalization detailed in [21], Fig. 14 gives schematic diagram of the sixth-order in-line

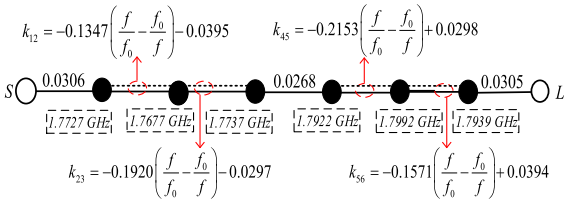

FIGURE 14. Resonating frequencies and circuit couplings for the sixth-order in-line topology filter in band-pass domain.

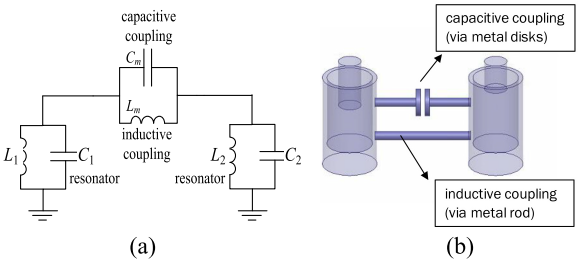

FIGURE 15. Realization of FVC by parallel-connected resonant structure. (a) Circuit model; (b) EM model, where the diameter of metal disks d_c and height of metal rod h_l are adjusted to obtain a required FVC value.

filter in the band-pass domain, where all the coupling values as well as resonant frequencies are provided.

Specifically, direct-coupled FVCs, i.e., k_{12}, k_{23}, k_{45}, and k_{56}, are described as

$$k_{i,i+1} = C_{i,i+1}\left(\frac{f}{f_0} - \frac{f_0}{f}\right) + k_{0,i,i+1}, \quad i = 1, 2, 4, 5 \tag{16}$$

which are related to the frequency parameter f. Note that, a TZ is generated in the band-pass domain by each FVC at

$$f_{zi} = \frac{f_0}{2C_{i,i+1}}\left(-k_{0,i,i+1} + \sqrt{\left(k_{0,i,i+1}\right)^2 + 4C_{i,i+1}^2}\right) \tag{17}$$

Moreover, all the frequency slopes $C_{i,i+1}$ are manipulated to be negative in Fig. 14 (as in-line configuration is concerned, this can be done simply by changing the sign of both $C_{i,i+1}$ and $M_{i,i+1}$ if $C_{i,i+1}$ is positive [16]); it implies that these variant couplings can be realized via the same kind of physical structure during implementation. Additionally, it is observed that $C_{i,i+1}$ and $k_{0,i,i+1}$ of each variant coupling are with the same sign symbol when the generated TZ is below f_0, while $C_{i,i+1}$ and $k_{0,i,i+1}$ are in opposite sign symbols when the TZ is above f_0.

In accordance with the mechanism discussed in [22] and [24], an FVC is practically implemented via parallel-connected resonant structure as Fig. 15 illustrates, whose coupling coefficient is represented as K. Note that, K is a mixed coupling that incorporates both capacitive coupling (by the metal disks) and inductive coupling (by the metal rod) as an entity. The desired $k_{i,i+1}$ of an FVC is thus approximately realized under two requirements:

1) The resonant structure provides desired coupling value at the center frequency, i.e., $K = k_{i,i+1}(f_0)$;
2) The structure resonates at the desired TZ location, i.e., $f_{zi} = 1/\sqrt{L_m C_m}$ for the ith variant coupling.

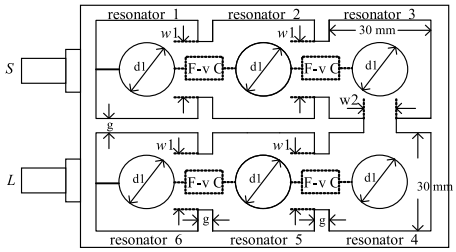

(a)

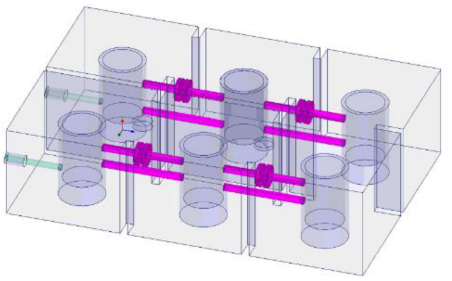

(b)

FIGURE 16. (a) Top view schematic and (b) EM model of the sixth-order coaxial cavity filter. The related dimensions are $d1 = 12$ mm, $g = 2$ mm, $w1 = 20$ mm, and $w2 = 16$ mm. Diameters of metal disks for each FVC (denoted as dashed box) are $d_{c1} = 3.1$ mm, $d_{c2} = 3$ mm, $d_{c3} = 3$ mm, $d_{c4} = 2.9$ mm, while heights of metal rod for each FVC are $h_{l1} = 6.9$ mm, $h_{l2} = 7.7$ mm, $h_{l3} = 9.5$ mm, $h_{l4} = 10.1$ mm.

To satisfy these requirements, the diameter of metal disks d_c and height of metal rod h_l of a resonant structure are properly combined during simulation, whose procedure has been detailed in [22].

With above discussions, the sixth-order filter is then modeled by using coaxial cavities as Fig. 16 depicts. Without any cross-coupling, the resonators are placed in two rows conveniently. Note that, each resonator is comprised by a metal box (with dimensions 30 mm × 30 mm × 25 mm) as well as a metal cylinder (with $d_1 = 12$ mm in diameter and $h = 21$ mm in height).

After some adjustment, the diameter of metal disks (represented as $d_{c,i}$) and the height of metal rods (represented as $h_{l,i}$) to realize the ith FVC (denoted as F-v C in Fig. 16(a)) are selected as $d_{c1} = 3.1$ mm, $h_{l1} = 6.9$ mm,$d_{c2} = 3$ mm, $h_{l2} = 7.7$ mm,$d_{c2} = 3$ mm, $h_{l3} = 9.5$ mm, and $d_{c4} = 2.9$ mm, $h_{l4} = 10.1$ mm. On the other hand, constant coupling between resonator 3 and 4 is mainly determined by the width $w2$ of the inductive window (see Fig. 16(a)), which is stipulated as $w_2 = 16$ mm in simulation. Additionally, the input and output couplings are generated by tapped-in metal lines, whose diameter is 1.2 mm and respective heights are $h_s = 7.28$ mm and $h_l = 6.74$ mm.

A photograph of the fabricated sixth-order in-line filter is given in Fig. 17, occupying a total area of 67 mm × 99 mm × 29 mm.

The EM simulation (by HFSS) and measured results of the sixth-order example are proposed in Fig. 18, both of which show a desired center frequency at $f_0 = 1.7825$ GHz and a bandwidth of $BW = 85$ MHz. Moreover, S_{11} is found below

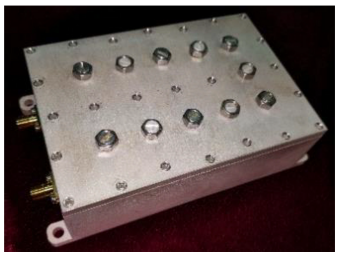

FIGURE 17. Photograph of the fabricated sixth-order in-line filter (with top lid). Note that metal rods above the resonators and coupling structures are implemented for the tuning.

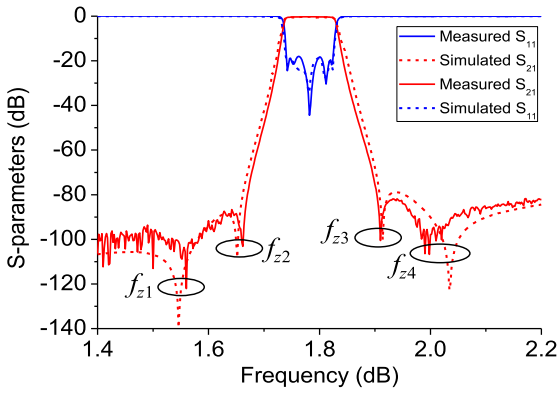

FIGURE 18. EM simulation and measured results for the sixth-order in-line coaxial resonator filter.

−20 dB (or −19 dB) within the whole passband in simulation (or measurement), which satisfies the return loss requirement. On the other hand, the TZs under simulation are located at $f_{z1} = 1.54$ GHz, $f_{z2} = 1.65$ GHz, $f_{z3} = 1.91$ GHz, $f_{z4} = 2.02$ GHz, respectively, while those of the measured results become $f_{z1} = 1.56$ GHz, $f_{z2} = 1.66$ GHz, $f_{z3} = 1.91$ GHz, $f_{z4} = 2$ GHz, which are very close to the desired locations and considered acceptable.

VI. CONCLUSION

A direct synthesis approach that can realize in-line topology narrowband filters comprising adjacent frequency-variant couplings is presented in this paper. Based on a general and deterministic process to manipulate a frequency-variant quadruplet, it has been shown that a maximum number of $N - 1$ transmission zeros (this is the most number available without source-load coupling) is achievable for an Nth-order cascaded network, which shows distinct improvement with regard to previous works. Generating each frequency-variant coupling via a single transformation matrix, this work also exhibits great benefit in the transformation simplicity.

REFERENCES

[1] S. Tamiazzo and G. Macchiarella, "An analytical technique for the synthesis of cascaded N-tuplets cross-coupled resonators microwave filters using matrix rotations," *IEEE Trans. Microw. Theory Techn.*, vol. 53, no. 5, pp. 1693–1698, May 2005.

[2] R. J. Cameron, "Advanced coupling matrix synthesis techniques for microwave filters," *IEEE Trans. Microw. Theory Techn.*, vol. 51, no. 1, pp. 1–10, Jul. 2003.

[3] R. J. Cameron, "General coupling matrix synthesis methods for Chebyshev filtering functions," *IEEE Trans. Microw. Theory Techn.*, vol. 47, no. 4, pp. 433–442, Apr. 1999.

[4] Y. He, G. Wang, X. Song, and L. Sun, "A coupling matrix and admittance function synthesis for mixed topology filters," *IEEE Trans. Microw. Theory Techn.*, vol. 64, no. 12, pp. 4444–4454, Dec. 2016.

[5] S. Tamiazzo and G. Macchiarella, "Synthesis of cross-coupled prototype filters including resonant and non-resonant nodes," *IEEE Trans. Microw. Theory Techn.*, vol. 63, no. 10, pp. 3408–3415, Oct. 2015.

[6] O. Glubokov and D. Budimir, "Extraction of generalized coupling coefficients for inline extracted pole filters with nonresonating nodes," *IEEE Trans. Microw. Theory Techn.*, vol. 59, no. 12, pp. 3023–3029, Dec. 2011.

[7] W. Menzel and M. Berry, "Quasi-lumped suspended stripline filters with adjustable transmission zeroes," in *IEEE MTT-S Int. Microw. Symp. Dig.*, Jun. 2004, pp. 1601–1604.

[8] S. Amari and J. Bornemann, "Using frequency-dependent coupling to generate finite attenuation poles in direct-coupled resonator bandpass filters," *IEEE Microw. Guided Wave Lett.*, vol. 9, no. 10, pp. 404–406, Oct. 1999.

[9] M. Politi and A. Fossati, "Direct coupled waveguide filters with generalized Chebyshev response by resonating coupling structures," in *Proc. Eur. Microw. Conf. (EuMC)*, Sep. 2010, pp. 966–969.

[10] L. Szydlowski, A. Jedrzejewski, and M. Mrozowski, "A trisection filter design with negative slope of frequency-dependent crosscoupling implemented in substrate integrated waveguide (SIW)," *IEEE Microw. Wireless Compon. Lett.*, vol. 23, no. 9, pp. 456–458, Sep. 2013.

[11] A. Jedrzejewski, L. Szydlowski, and M. Mrozowski, "Accurate design of pseudoelliptic inline SIW filters with frequency-dependent couplings," in *Proc. 20th IEEE Int. Conf. Microw., Radar, Wireless Commun. (MIKON)*, Jun. 2014, pp. 1–4.

[12] S. Bastioli, R. V. Snyder, and P. Jojic, "High power in-line pseudoelliptic evanescent mode filter using series lumped capacitors," in *Proc. 41st Eur. Microw. Conf. (EuMC)*, Oct. 2011, pp. 87–90.

[13] Q.-X. Chu and H. Wang, "A compact open-loop filter with mixed electric and magnetic coupling," *IEEE Trans. Microw. Theory Techn.*, vol. 56, no. 2, pp. 431–439, Feb. 2008.

[14] L. Szydlowski, A. Lamecki, and M. Mrozowski, "Coupled-resonator waveguide filter in quadruplet topology with frequency-dependent coupling—A design based on coupling matrix," *IEEE Microw. Wireless Compon. Lett.*, vol. 22, no. 11, pp. 553–555, Nov. 2012.

[15] L. Szydlowski and M. Mrozowski, "A self-equalized waveguide filter with frequency-dependent (resonant) couplings," *IEEE Microw. Wireless Compon. Lett.*, vol. 24, no. 11, pp. 769–771, Nov. 2014.

[16] Y. He and N. Yoshikawa, "Notes on determination of frequency-variant coupling for high selectivity in-line filters," in *Proc. Asia–Pacific Microw. Conf. (APMC)*, Kyoto, Japan, Nov. 2018, pp. 100–102.

[17] P. Kozakowski, A. Lamecki, M. Mongiardo, M. Mrozowski, and C. Tomassoni, "Computer-aided design of in-line resonator filters with multiple elliptical apertures," in *IEEE MTT-S Int. Microw. Symp. Dig.*, Jun. 2004, pp. 611–614.

[18] N. Leszczynska, L. Szydlowski, and M. Mrozowski, "A novel synthesis technique for microwave bandpass filters with frequency-dependent couplings," *Prog. Electromagn. Res.*, vol. 137, pp. 35–50, May 2013.

[19] L. Szydlowski, A. Lamecki, and M. Mrozowski, "Coupled-resonator filters with frequency-dependent couplings: Coupling matrix synthesis," *IEEE Microw. Wireless Compon. Lett.*, vol. 22, no. 6, pp. 312–314, Jun. 2012.

[20] S. Amari, M. Bekheit, and F. Seyfert, "Notes on bandpass filters whose inter-resonator coupling coefficients are linear functions of frequency," in *IEEE MTT-S Int. Microw. Symp. Dig.*, Atlanta, GA, USA, Jun. 2008, pp. 1207–1210.

[21] S. Tamiazzo and G. Macchiarella, "Synthesis of cross-coupled filters with frequency-dependent couplings," *IEEE Trans. Microw. Theory Techn.*, vol. 65, no. 3, pp. 775–782, Mar. 2017.

[22] Y. He *et al.*, "A direct matrix synthesis for in-line filters with transmission zeros generated by frequency-variant couplings," *IEEE Trans. Microw. Theory Techn.*, vol. 66, no. 4, pp. 1780–1789, Apr. 2018.

[23] J.-S. Hong and M. J. Lancaster, *Microstrip Filters for RF/Microwave Applications*. New York, NY, USA: Wiley, 2001.

[24] H. Wang and Q. X. Chu, "An inline coaxial quasi-elliptic filter with controllable mixed electric and magnetic coupling," *IEEE Trans. Microw. Theory Techn.*, vol. 57, no. 3, pp. 667–673, Mar. 2009.

YUXING HE (S'15–M'18) received the B.S. and Ph.D. degrees in electrical engineering from the University of Science and Technology of China, Hefei, China, in 2008 and 2017, respectively. Since 2017, he has been a Visiting Researcher with the Dipartimento di Elettronica, Informazione e Bioingegneria, Politecnico di Milano, Italy.

He is currently a specially assigned Assistant Professor with the Institute of Advanced Sciences, Yokohama National University, Yokohama, Japan. His research interests involve microwave & RF passive circuit design, advanced synthesis techniques for high performance filters & multiplexers, and their applications on low-temperature superconducting logic circuits.

He has served on the Review Board of the IEEE TRANSACTIONS ON MICROWAVE THEORY AND TECHNIQUES and the IEEE MICROWAVE AND WIRELESS COMPONENTS LETTERS.

GIUSEPPE MACCHIARELLA (M'90–SM'06–F15) received the Laurea degree in electronic engineering from the Politecnico di Milano, Italy, in 1975. From 1977 to 1985, he was with the National Research Council, where he was involved in the SIRIO propagation experiment (First Italian Satellite for Telecommunication).

He is currently a Professor of microwave engineering with the Department of Electronic, Information and Bioengineering, Politecnico di Milano. His research activity has covered in the past several areas of microwave engineering: microwave acoustics (SAW devices), radio wave propagation, numerical methods for electromagnetic, power amplifiers, and linearization techniques. He has been a Scientific Coordinator of PoliEri, a Research Laboratory on monolithic microwave integrated circuit, which was jointly supported by the Politecnico di Milano and Ericsson Company. He has authored or coauthored more than 150 papers on journals and conferences proceedings. He has been responsible of several contracts and collaborations with various Companies operating in the microwave industry. His current research interests include the development of new techniques for the synthesis of microwave filters and multiplexers.

From 2017 to 2019, he was the Chair of the IEEE Technical Committee MTT-8 (Filters and Passive Components). He is serving since several years in the Technical Program Committee of the IEEE International Microwave Symposium and European Microwave Conference.

ZHEWANG MA (S'91–M'96) received the B.Eng. and M.Eng. degrees from the University of Science and Technology of China, Hefei, China, in 1986 and 1989, respectively. In 1995, he was granted the Dr.Eng. degree from the University of Electro-Communications, Tokyo, Japan. He was a Research Assistant with the Department of Electronic Engineering, University of Electro-Communications, in 1996, where he became an Associate Professor, in 1997. From 1998 to 2008, he was an Associate Professor with the Department of Electrical and Electronic Systems, Saitama University, Japan, where he was a Professor, in 2009. From 1985 to 1989, he was engaged in research works on dielectric waveguides, resonators, and leaky-wave antennas. From 1990 to 1997, he did studies on computational electromagnetics, analytical, and numerical modeling of various microwave and millimeter wave transmission lines and circuits. His current research interests include the development of microwave and millimeter-wave devices and circuits, measurements of dielectric materials, and high temperature superconductors.

He is a Senior Member of the Institute of Electronics, Information and Communication Engineers (IEICE) of Japan. He was a member of the Steering and/or Technical Committees of the Asia Pacific Microwave Conference. From 1994 to 1996, he was a Research Fellow of the Japan Society for the Promotion of Science. He received the Japanese Government Graduate Scholarship, from 1991 to 1993. He was granted the URSI Young Scientist Award, in 1993. He received the CJMW Microwave Prize, in 2008 and 2011. He was also a recipient of the Best Paper Award from IEICE, in 2018. He has served on the Editorial Board of the IEEE TRANSACTIONS ON MICROWAVE THEORY AND TECHNIQUES, on the Review Board of the IEEE MICROWAVE AND WIRELESS COMPONENTS LETTERS, the *International Journal of RF and Microwave Computer-Aided Engineering*, *IEICE Transactions on Electronics*, Japan, and as an Editor of two Special Issues of *IEICE Transactions on Electronics*. He is the Vice President of the Technical Group on Electronics Simulation Technology of the Electronics Society, IEICE.

LIGUO SUN was born in Fuyang, Anhui, China, in 1960. He received the B.S. and Ph.D. degrees in electrical engineering from the University of Science and Technology of China (USTC), Hefei, Anhui, China, in 1982 and 1991, respectively, and the M.S. degree in electrical engineering from the China Research Institute of Radio Wave Propagation, Xinxiang, Henan, China, in 1985. From 1985 to 1988, he was an Engineer with the Research Center, China Research Institute of Radio Wave Propagation, Qingdao, Shandong, China. From 1991 to 1995, he was an Associate Research Fellow with the Institute of Remote Sensing Application, Chinese Academy of Sciences, Beijing, China. From 1995 to 1996, he was with the Massachusetts Institute of Technology, Cambridge, MA, USA, and Northeast University, Boston, MA, USA, as a Senior Visiting Scholar. From 1996 to 2000, he was a Senior Engineer and a Manager with DSC Ltd., Tyco International Ltd., Toronto, ON, Canada. From 2000 to 2009, he was a Senior Staff Engineer with Sychip, Inc., Murata Manufacturing Company, Ltd., Dallas, TX, USA. Since 2009, he has been a Full Professor with USTC. His research interests include RF circuits, devices, and system integration, signal integrity, antenna, electromagnetic wave propagation and scattering, microwave remote sensing, and dielectric waveguide.

NOBUYUKI YOSHIKAWA received the B.E., M.E., and Ph.D. degrees in electrical and computer engineering from Yokohama National University, Japan, in 1984, 1986, and 1989, respectively. Since 1989, he has been with the Department of Electrical and Computer Engineering, Yokohama National University, where he is currently a Professor. His research interests include superconductive devices and their application in digital and analog circuits, single-electron-tunneling devices, quantum computing devices, and cryo-CMOS devices.

Dr. Yoshikawa is a member of the Institute of Electronics, Information and Communication Engineers of Japan, the Japan Society of Applied Physics, the Institute of Electrical Engineering of Japan, Cryogenics and Superconductivity Society of Japan, and the Institute of Electrical and Electronics Engineers.